Synthesis and Characterization of Heterometallic Iron–Uranium Complexes with a Bidentate N-Donor Ligand (2,2′-Bipyridine or 1,10-Phenanthroline)

Schöne, S.; Radoske, T.; März, J.; Stumpf, T.; Ikeda-Ohno, A.;

Originally published:

October 2018

Inorganic Chemistry 57(2018)21, 13318-13329

DOI: https://doi.org/10.1021/acs.inorgchem.8b01868

Synthesis and Characterization of Hetero-metallic Iron-Uranium Complexes with a Bidentate N-donor Ligand (2,2'-Bipyridine or 1,10-Phenanthroline)

*Sebastian Schöne, Thomas Radoske, Juliane März, Thorsten Stumpf, and Atsushi Ikeda-Ohno**

Helmholtz-Zentrum Dresden-Rossendorf, Institute of Resource Ecology, Bautzner Landstrasse 400, 01328 Dresden, Germany

(* corresponding author, E-mail: a.ikeda@hzdr.de)

ABSTRACT. The coordination chemistry of the diamine ligands, 2,2'-bipyridine (bipy) and 1,10-phenanthroline (phen), with *d*- and *f*-block metals has been extensively explored during the last century to yield many technological and industrial applications. Despite this long history, the chemistry of these diamine ligands in hetero-metallic systems containing multiple metals is poorly understood even to date. This study reports, for the first time, a systematic investigation into the coordination behavior bipy/phen in the hetero-metallic iron-uranium system covering all the combination of the possible redox couples (i.e. Fe^{2+}/Fe^{3+} and U^{4+}/U^{6+}) that are potentially relevant to the actual engineered or environmental systems. In total, eleven new compounds of pure-uranium and hetero-metallic Fe-U complexes were successfully synthesized and structurally characterized. The synthesized compounds show an intriguing structural variety in terms of the nuclearity of the metal center (mono- and dinuclear for both Fe and U) and the manner of crystal packing based on different intra- and intermolecular interactions (e.g. π···π interactions, hydrogen bonding, etc.). The results also highlight the similarity of the fundamental coordination properties of bipy and phen towards Fe and U, regardless of the oxidation states of the metals, as well as the striking dissimilarity in their chemical behavior upon crystal packing.

1. INTRODUCTION

Owing to their remarkable coordination ability towards a wide range of metal ions with various oxidation states, the bidentate N-donor ligands of 2,2'-bipyridine (bipy) and 1,10-phenanthroline (phen) have been attracting considerable interests in the coordination chemistry of *d*- and *f*-block elements, for instance in the fields of organometallic and supramolecular chemistry,[1-4] catalysis[5-6] and photoelectrochemistry.[7-8] Furthermore, the bipy/phen complexes with some transition metals could be of particular importance in biochemistry for probing and manipulating DNA[9-11] as well as for medical applications.[12]

The constant and unflagging applications of bipy and phen ligands attribute largely to the remarkable stability of metal complexes with these diamine ligands. This stability stems from the presence of two N-donor atoms in juxtaposition with a suitable N-N distance, materializing a rigid bidentate coordination[13] as well as the ligands' aromaticity involving σ-/π- donor and π^*-acceptor orbitals that enhance the electronic interaction with the metal centers.[8] The coordination of two or three of these bidentate ligands completely occupies the primary coordination sphere of the metal center,[14] leading to stable metal complexes with versatile chromatic properties for a wide variety of analytical applications.[15]

Among the metal-bipy complexes investigated thus far, the tris(bipyridine) iron(II) complex ($[Fe(bipy)_3]^{2+}$) is the first complex of this type,[16] which has been synthesized only a few years after the discovery of bipy in 1889 by Fritz Blau.[17] Even more than a century after the discovery, the iron complexes with bipy are still being one of the most attractive subjects of coordination chemistry, which can be demonstrated by the recent discovery of small molecular knots based on iron-bipy interactions,[18] for instance. Due to its unique electronic properties originating from the spin crossover (SCO) transition, the $[Fe(bipy)_3]^{2+}$ complex also possesses a huge potential for functional materials, such as magnetic or electronic devices.[19-20]

The tris(phenanthroline) iron(II) complex ($[Fe(phen)_3]^{2+}$), which is an analogue of $[Fe(bipy)_3]^{2+}$ and also known as ferroin, is one of the most common redox indicators used in analytical chemistry.[21] This is due to the remarkable stability of the $[Fe(phen)_3]^{2+}$ complex in aqueous solutions as compared with a pure aquo species of Fe(II) which is redox-sensitive and, therefore, not stable under normal atmospheric conditions. The stability of the $[Fe(phen)_3]^{2+}$ complex is substantiated by a significant increase in the standard redox potential between Fe^{2+}/Fe^{3+}- and $[Fe(phen)_3]^{2+}/[Fe(phen)_3]^{3+}$ couples (0.771 V and 1.147 V, respectively).[22] Additionally, the ($[Fe(phen)_3]^{2+}$ complex has recently attracted another attention as a potential candidate for optical switches in non-linear optics.[23]

Despite a large number of precedent studies on the metal complexes with bipy and phen ligands, as represented by the iron complexes mentioned above, the bipy/phen complexes containing multiple metals have been explored surprisingly little. Such multi-metal systems would be more relevant to the actual engineered or environmental systems where different elements coexist, suggesting that the investigations into the hetero-metallic complexes of bipy/phen would further expand the potential of these versatile ligands not only for fundamental research but also for their technological and industrial applications. This motivates us to perform the present study focusing on the chemical behavior of bipy/phen in the presence of two different metals, namely iron (Fe) and uranium (U). The combination of these two metals is of particular importance for the understanding of the behavior of these metals under the geochemical conditions relevant to uranium mining or radioactive waste disposal,[24-26] where both iron and uranium are abundant in the systems. Additionally, both iron and uranium are redox-active metals (i.e. Fe^{2+}/Fe^{3+} and U^{4+}/U^{6+}, respectively), potentially forming a variety of different redox couples under normal aqueous conditions. This also indicates that the coexistence of multiple redox-active metals complicates not only the coordination behavior of the metals but also their redox behavior. For

instance, it has been reported that the reduction behavior of uranium by zero-valent iron (ZVI), a promising reductant for the treatment of uranium-contaminated water,[27-29] is significantly affected by the presence of phen.[30] This suggests the potential importance of the hetero-metallic Fe-U complexes with bipy/phen in terms of environmental chemistry, in addition to fundamental chemical interest. The coordination chemistry of the hetero-metallic Fe-U system has been investigated in the presence of inorganic anions,[31-34] carboxylates,[35-37] and other organic ligands.[38] These precedent studies, however, focus solely on the U(VI) complexes (as uranyl(VI): UO_2^{2+}), and none of them address the potential complexity associated with the interaction of the two redox-active metals.

Given these backgrounds, this study aims to systematically investigate the hetero-metallic Fe-U system in the presence of bipy or phen. All the possible combinations of Fe(II)/Fe(III), U(IV)/U(VI) and bipy/phen are attempted in an aqueous solution to obtain possible complexes as a solid product. The obtained solid products are characterized mainly by single-crystal- and powder X-ray diffraction to elucidate their coordination and structural properties. The obtained results are further discussed particularly in terms of the chemical similarity or dissimilarity between Fe(II) and –(III), U(IV) and –(VI), and bipy and phen.

2. EXPERIMENTAL SECTION

Caution! Natural uranium consists of radioactive nuclides including long-lived α-emitters (^{235}U; $T_{1/2} = 7.04 \times 10^8$ years, and ^{238}U; $T_{1/2} = 4.47 \times 10^9$ years) and is also chemically toxic. Special precautions as well as appropriate equipment and facilities for radiation protection are required for handling this material.

2.1. Synthesis of compounds

Materials. Starting compounds of uranium(IV) tetrachloride (UCl_4) and uranyl(VI) dichloride hydrate ($UO_2Cl_2 \cdot nH_2O$) were prepared as follows. UCl_4 was prepared from uranyl(VI) nitrate hexahydrate ($UO_2(NO_3)_2 \cdot 6H_2O$) and hexachloropropene (Sigma-Aldrich, > 90%) according to the procedure reported in literature,[39] while $UO_2Cl_2 \cdot nH_2O$ was prepared by dissolving $UO_3 \cdot mH_2O$ in a concentrated hydrochloric acid followed by evaporation of the solvents.[40] PXRD measurements on the resultant compounds revealed that UCl_4 consists of a pure phase, whereas $UO_2Cl_2 \cdot nH_2O$ is a mixture of $UO_2Cl_2 \cdot 3H_2O$ and $UO_2Cl_2 \cdot 1H_2O$. Additional thermogravimetric analysis underlines these findings (see Section 1 in the Supporting Information (SI)). Pure uranyl(VI) compounds were synthesized by dissolving $UO_2Cl_2 \cdot nH_2O$ in degassed and deionized water and addition of either 2,2'-bipyridine (bipy) (Carl Roth, 95%) or 1,10-phenanthroline (phen) monohydrate (Merck, 99.5%) in degassed acetone. Due to the limited solubility of bipy and phen in water, these ligands were always dissolved in degassed acetone in this study. The iron-uranyl(VI) compounds were prepared by dissolving $UO_2Cl_2 \cdot nH_2O$ and either iron(II) chloride ($FeCl_2$, Sigma-Aldrich, 98%) or iron(III) chloride ($FeCl_3$, Sigma-Aldrich, 99%) in degassed and deionized water. The sample solution was then mixed with a solution of bipy or phen monohydrate in degassed acetone. The iron-uranium(IV) compounds were prepared by dissolving UCl_4 and $FeCl_2$ in degassed water followed by the addition of either bipy or anhydrous

phen (Alfa Aesar, 99%) dissolved in degassed acetone. All preparations were performed in an inert glove box filled with N_2 or using Schlenk techniques. All the chemicals except the uranium compounds were commercial products and used as received without further purification. The solvents were degassed using freeze-thaw cycles.

*[UO_2(bipy)Cl_2(H_2O)] (**1**).* 186 mg of $UO_2Cl_2 \cdot nH_2O$ (0.5 mmol) was dissolved in 2 mL of degassed water, and a 2 mL of acetone solution containing 77 mg of bipy (0.493 mmol) were gently added. The resulting yellow solution was then slowly evaporated at 30 °C. This resulted in the formation of yellow crystals on the surface of the sample vial. The crystalline precipitate was washed with tetrahydrofuran (THF) and dried at room temperature. 98% yield. The powder X-ray diffraction (PXRD) pattern of the resultant precipitate is given in Figure S4 in the SI. Elemental analysis: Calcd. for $C_{10}H_{10}Cl_2N_2O_3U$; C 23.3 H 2.0 N 5.4, found; C 23.6 H 1.9 N 5.4. IR (cm^{-1}): 734 (w), 746 (w), 771 (s), 892 (w), 904 (s), 928 (vs, ν_{as}(O=U=O)), 1006 (m), 1017 (m), 1316 (m), 1436 (m), 1475 (m), 1598 (m), 3327 (m).

*[(UO_2(bipy)Cl)$_2$(μ_2-OH)$_2$] (**2**).* A 1 mL of 0.1 M U(VI) in degassed water (149 mg of $UO_2Cl_2 \cdot nH_2O$ in 4 mL degassed water) were gently added to 3 mL of 0.1 M bipy in acetone (U:bipy = 1:3). This resulted in a color change from colorless to yellow. The solution was then slowly evaporated at 60 °C, yielding crystalline yellow precipitate. The powder X-ray diffraction (PXRD) measurement on the product (Fig. S5 in the SI) revealed that the precipitate is a mixture of **1** and **2**. The mixture of **1** and **2** was also produced when two equivalents of bipy were mixed with the UO_2Cl_2 solution. Other attempts to obtain a pure phase of **2** are not successful thus far. For these reasons, no additional characterization (i.e. elemental analysis and IR measurements) was performed on this compound.

*[(UO_2(phen)Cl)$_2$(μ_2-OH)$_2$]·2H_2O (**3**).* A 1 mL of 0.1 M UO_2Cl_2 in degassed water (149 mg of UO_2Cl_2·nH_2O in 4 mL degassed H_2O) were gently added to 2 mL of 0.1 M phen solution in acetone (U:phen = 1:2). This resulted in an immediate formation of yellow precipitate. After the precipitate was settled at the bottom of the sample vial, the supernatant was decanted and slowly evaporated at 60 °C. This resulted in a crystalline yellow precipitate in a very low yield that prevented further characterization with additional methods.

*[Fe(bipy)$_3$][UO_2Cl_4] (**4**).* A solution containing 234 mg of bipy (1.498 mmol) in 2 mL of acetone was gently added to a solution containing 187 mg of UO_2Cl_2·nH_2O (0.503 mmol) and 63 mg of $FeCl_2$ (0.497 mmol) in 4 mL of degassed water, resulting in a color change from yellow to dark red. The solvent was evaporated under reduced pressure, yielding the final product as deep red powder with 83% yield. The powder X-ray diffraction (PXRD) pattern of the resultant precipitate is given in Figure S6 in the SI. Single crystals of **5** were obtained by dissolving the compound in deionized water and slowly evaporating the solvent. Elemental analysis: Calcd. for $C_{30}H_{24}Cl_4N_6O_2FeU$; C 38.5 H 2.5 N 9.0 Fe 6.0 U 25.4, found; C 35.5 H 2.6 N 8.3 Fe 5.9 U 26.0. IR (cm^{-1}): 730 (s), 733 (s), 748 (s), 759 (vs), 774 (s), 890 (m), 920 (vs, ν_{as}(O=U=O)), 1423 (m), 1429 (m), 1442 (s), 1462 (m), 1601 (m), 3065 (w).

*[Fe(phen)$_3$][UO_2Cl_4] (**5**).* A solution containing 299 mg of phen monohydrate (1.508 mmol) in 2 mL acetone was gently added to a solution containing 185 mg of UO_2Cl_2·nH_2O (0.498 mmol) and 63 mg of $FeCl_2$ (0.497 mmol) in 4 mL of degassed water. Similarly to the preparation of the analogous compound **4**, this resulted in a color change from yellow to dark red. The solvent was then evaporated under reduced pressure, yielding the final product as deep red powder in 81%

yield. The powder X-ray diffraction (PXRD) pattern of the resultant precipitate is given in Figure S7 in the SI. Single crystals of **5** were obtained by dissolving the compound in deionized water and slowly evaporating the solvent. Elemental analysis: Calcd. for $C_{36}H_{24}Cl_4N_6O_2FeU$; C 42.9 H 2.4 N 8.3 Fe 5.5 U 23.6, found; C 40.4 H 2.7 N 7.8 Fe 5.3 U 21.8. IR (cm^{-1}): 720 (vs), 767 (m), 773 (m), 840 (s), 907 (m, ν$_{as}$(O=U=O)), 936 (m), 1416 (m), 1422 (m), 2973 (vw).

[(Fe(bipy)$_2$Cl)$_2$O][UO$_2$Cl$_4$]·H$_2$O ***(6).*** A solution containing 312 mg of bipy (1.998 mmol) in 2 mL of acetone was gently added to a solution containing 186 mg of $UO_2Cl_2 \cdot nH_2O$ (0.500 mmol) and 162 mg of $FeCl_3$ (0.999 mmol) in 4 mL of degassed water, resulting in a color change from yellow to deep orange. The solvent was evaporated under reduced pressure, yielding the final product as brownish red powder with a nearly quantitative yield. The powder X-ray diffraction (PXRD) pattern of the resultant precipitate is given in Figure S8 in the SI. Single crystals of **6** were obtained by dissolving the compounds in deionized water and slowly evaporating the solvent. Elemental analysis: Calcd. for $C_{40}H_{34}Cl_6N_8O_4Fe_2U$; C 38.4 H 2.6 N 9.0 Fe 9.0 U 19.0, found; C 36.8 H 2.8 N 8.5 Fe 9.0 U 17.5. IR (cm^{-1}): 655 (s), 731 (s), 764 (vs), 775 (s), 783 (w), 899 (m), 903 (m), 912 (m), 919 (vs, ν$_{as}$(O=U=O)), 1015 (m), 1021 (s), 1029 (w), 1105 (w), 1156 (m), 1173 (w), 1244 (w), 1312 (s), 1440 (s), 1470 (m), 1493 (w), 1565 (w), 1573 (w), 1600 (m), 3070 (w).

[(Fe(phen)$_2$Cl)$_2$O][UO$_2$Cl$_4$] ***(7).*** A solution containing 397 mg of phen monohydrate (2.003 mmol) in 2 mL of acetone was gently added to a solution containing 186 mg of $UO_2Cl_2 \cdot nH_2O$ (0.500 mmol) and 160 mg of $FeCl_3$ (0.986 mmol) in 4 mL of degassed water. Similarly to the preparation of the analogous compound of **6**, this resulted in a color change from yellow to deep orange. The solvent was then evaporated under reduced pressure, yielding the

final product as brownish red powder in 76% yield. The powder X-ray diffraction (PXRD) pattern of the resultant precipitate is given in Figure S9 in the SI. Single crystals of **7** were obtained by dissolving the compound in deionized water and slowly evaporating the solvent. Elemental analysis: Calcd. for $C_{48}H_{32}Cl_6N_8O_3Fe_2U$; C 43.3 H 2.4 N 8.4 Fe 8.4 U 17.9, found; C 42.1 H 3.3 N 8.1 Fe 8.1 U 17.4. IR (cm^{-1}): 699 (m), 721 (vs), 770 (w), 781 (w), 832 (s), 846 (vs), 867 (m), 914 (s), 1105 (w), 1424 (s), 1494 (w), 1516 (m), 1577 (w), 3042 (w).

*$[Hbipy]_2[UCl_6]$ (**8**)*. A 1 mL of 0.1 M bipy solution (94 mg of bipy in 6 mL of acetone) in acetone was added gently to a 1 mL of a solution containing 228 mg of 0.1 M UCl_4 in degassed water. This resulted in the formation of blueish gray precipitate at the interface between the two solutions. The sample solution was then stirred to obtain a clear turquois solution, and the solution was evaporated at 30 °C to obtain compound **8**. The PXRD measurement revealed that the final product consists of a pure phase of **8** (Figure S10 in the SI). Single crystals of compound **8** could be also obtained by dissolving UCl_4 and bipy in dimethoxyethane separately, and letting the two solutions diffuse into one another gently. Elemental analysis: Calcd. for $C_{20}H_{18}Cl_6N_4U$; C 31.3 H 2.4 N 7.3, found; C 24.6 H 1.9 N 5.1. IR (cm^{-1}): 724 (s), 743 (s), 759 (vs), 766 (s), 868 (m), 925 (m), 984 (w), 993 (w), 1086 (m), 1154 (m), 1168 (w), 1218 (w), 1280 (w), 1307 (w), 1319 (w), 1431 (m), 1455 (m), 1470 (m), 1528 (s), 1571 (w), 1586 (s), 1603 (m), 1617 (w), 2923 (w), 3104 (w).

*$[Hphen]_2[UCl_6]$ (**9**)*. A 1 mL of 0.1 M phen monohydrate in acetone was gently added to a 1 mL of a solution containing 0.1 M UCl_4 in degassed water. Similarly to the preparation of the analogous compound **8**, this resulted in the formation of blueish gray precipitate at the interface between the two solutions. The sample solution was then stirred to obtain a clear turquois

solution, and the solution was evaporated at 30°C. This resulted in the formation of small green crystals. The PXRD measurement revealed that the final product consists of a pure phase of **9** (Figure S11 in the SI). Single crystals of compound **9** were also obtained as a by-product in the synthesis of compound **11**. Elemental analysis: Calcd. for $C_{24}H_{18}Cl_6N_4U$; C 35.4 H 2.2 N 6.9, found; C 27.8 H 2.0 N 5.0. IR (cm^{-1}): 715 (vs), 777 (m), 817 (m), 844 (vs), 1185 (m), 1417 (m), 1450 (m), 1466 (s), 1493 (m), 1538 (vs), 1584 (s), 1594 (vs), 1615 (m), 2854 (m), 2921 (m), 3204 (w).

*$[Fe(bipy)_3][UCl_6]$ (**10**).* 2 mL of a solution containing 189.9 mg of UCl_4 dissolved in 10 mL degassed water ([U] = 0.05 M) were first mixed with 2 mL of a solution containing 68.0 mg of $FeCl_2$ in 10 mL degassed water ([Fe] = 0.05 M), and the resultant mixture was then gently added to 6 mL of 0.05 M bipy solution in acetone. This resulted in a color change from blue-gray to deep red. The solution was then slowly evaporated at 40 °C. This resulted in the formation of red precipitate together with some deep red crystals. The powder X-ray diffraction (PXRD) pattern of the resultant precipitate is given in Figure S12 in the SI. Elemental analysis: Calcd. for $C_{30}H_{24}Cl_6N_6FeU$; C 36.9 H 2.5 N 8.6 Fe 5.7 U 24.4, found; C 37.0 H 2.4 N 8.6 Fe 6.2 U 24.4. IR (cm^{-1}): 658 (w), 731 (s), 762 (s), 773 (s), 1158 (w), 1312 (w), 1425 (m), 1439 (m), 1464 (m), 1602 (m), 3068 (w).

*$[Fe(phen)_3][UCl_6]$ (**11**).* 190 mg of UCl_4 (0.5 mmol) and 63 mg of $FeCl_2$ (0.497 mmol) were dissolved in 4 mL of degassed water, yielding a clear blue-gray solution. This solution was transferred into a Schlenk flask, and gently mixed with a solution of 297 mg of anhydrous phen (1.5 mmol) in 4 mL of degassed acetone. This resulted in a color change from blue-gray to dark red. The solvent was then evaporated under reduced pressure, giving the final product as red

brown precipitate with 86% yield. The powder X-ray diffraction (PXRD) pattern of the resultant precipitate is given in Figure S13 in the SI. Single crystals of **11** with unsufficient quality could be obtained by recrystallization of the resultant precipitate in aqueous solution at 30°C. Elemental analysis: Calcd. for $C_{38}H_{32}Cl_6N_6O_2FeU$; C 41.0 H 2.5 N 7.6 Fe 5.0 U 21.4, found; C 41.4 H 2.3 N 7.9 Fe 5.2 U 21.3. IR (cm-1): 720 (s), 766 (w), 775 (w), 840 (m), 1407 (w), 1422 (w), 3053 (w).

2.2. Single-crystal X-ray diffraction (SC-XRD)

Crystals of compounds **1-11** were analyzed on a Bruker D8 Venture single-crystal x-ray diffractometer with micro-focused Mo Kα radiation (λ = 0.71073 Å) and a PHOTON 100 CMOS detector. All the data were collected at 100 K. Single crystals appropriate for the measurement were selected on an optical microscope equipped with a polarization filter, and mounted on a MicroMount™ supplied by MiTeGen, USA, with mineral oil. Generic φ- and ω-scans were performed to collect several sets of narrow data frames. Data treatment was performed with the Bruker APEX 3 program suite including the Bruker SAINT software package for integration.[41] Empirical absorption correction using the Multi-Scan method (SADABS[42]) was applied to the collected data. The structure was solved and refined with full-matrix least-squares data on F^2 using the Bruker SHELXTL[43] software package and the program ShelXle.[44] All non-hydrogen atoms were refined anisotropically. Hydrogen atoms of the phenyl rings were placed at calculated positions and allowed to ride on their parent atoms. Hirshfeld surfaces analysis[45-46] on the acquired crystal structure data and the visualization of results were performed using the software *CrystalExplorer* (Ver. 17.5).[47]

2.3. Powder X-ray diffraction (PXRD)

The purity of the obtained compounds **1-11** was confirmed by PXRD. The data were collected at ambient temperature on a Rigaku MiniFlex 600 equipped with Cu Kα radiation (λ = 1.54184 Å) and a D/Tex Ultra Si strip detector in the Bragg−Brentano geometry (θ–2θ mode). The compounds containing iron were measured with the X-ray fluorescence suppression mode on the D/Tex detector to minimize the effect of fluorescence X-rays from iron on the collected data.

2.4. Infra-red (IR) spectroscopy

IR spectra of compounds **1-11** were measured on an Agilent Cary 630 FT-IR spectrometer equipped with a single-reflection attenuated total reflection (ATR) accessory made of diamond. The measurements were performed in an inert glove box filled with N_2. The spectra were recorded between 4000 and 650 cm^{-1} with a resolution of 2 cm^{-1}.

2.5. Elemental analysis

Elemental analysis for H, C and N were performed on a vario MICRO cube (Elementar) with a helium gas flow.

2.6. Thermogravimetry and differential scanning calorimetry

Thermogravimetry and differential scanning calorimetry (TG-DSC) measurements were carried out on a STA 449F5 Jupiter (Netzsch) under synthetic air from room temperature (25 °C) up to 1000 °C with a heating rate of 20 °C/min.

3. RESULTS AND DISCUSSION

3.1. Hexavalent uranium (U(VI) as UO_2^{2+})

The hexavalent uranyl unit $[O=U=O]^{2+}$ is the predominant form of uranium under natural conditions. Due to the remarkable stability of the trans-dioxo uranium unit stemming from the involvement of "semi-core" 6p orbitals in the U–O bonding,[48-49] the coordination behavior of U(VI) is generally limited exclusively to the equatorial plane of the uranyl unit.[50]

3.1.1. Pure U(VI)-ligand system

Despite the extensive use of bipy/phen as surface capping agents for the metal organic frameworks (MOFs) based on uranyl ions and polycarboxylic acids,[51-54] the fundamental complexation behavior of these nitrogen-donor ligands toward uranyl ions has not been well described even to date.

Starting with a stoichiometric amount of U(VI) and bipy dissolved in a water/acetone mixture, the complex with a U:bipy stoichiometry of 1:1 ($[UO_2(bipy)Cl_2(H_2O)]$ (**1**)) was obtained (Figure 1-left). The U center in **1** is sevenfold coordinated, forming a slightly distorted pentagonal bipyramid around the U center. In addition to two "*yl*"-oxygens, two chlorides, two nitrogens of the bipy molecule, and one water molecule surround the U center. The two chlorides and the water molecule on the equatorial plane are positioned nearly perpendicularly to the "*yl*"-oxygens, while the bipy ligand is not coordinating on the equatorial plane. The dihedral angle between the N1–U–N2 and the Cl1–U–Cl2 planes is closed to 34°, indicating a significant distortion of the equatorial plane of the uranyl unit. Furthermore, the bipy ligand shows a significant torsion angle (N1–C5–C6–N2) of 15.3(8)°, which is comparable to the angles found in other mononuclear U(VI)-bipy complexes.[55-56] As discussed in detail below, the observed torsion angle of bipy molecules would reflect their geometrical flexibility upon crystallization.

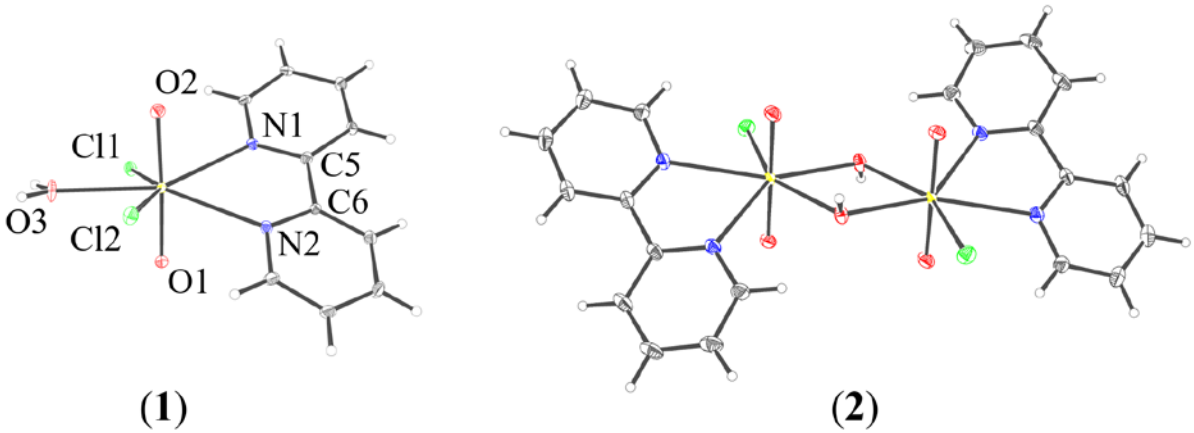

Figure 1. ORTEP plots of $[UO_2(bipy)Cl_2(H_2O)]$(**1**, left) and $[(UO_2(bipy)Cl)_2(\mu_2\text{-}OH)_2]$ (**2**, right). Thermal ellipsoids are drawn at 50% probability level. Color code: hydrogen (H, white), carbon (C, dark gray), chlorine (Cl, light green), nitrogen (N, blue), oxygen (O, red), and uranium (U as U^{6+}, yellow).

When increasing the U:bipy ratio to 1:2 under the same condition applied to the synthesis of **1**, the resultant precipitate was found to be composed of a mixture of **1** and another dinuclear complex of $[(UO_2(bipy)Cl)_2(\mu_2\text{-}OH)_2]$ (**2**) (Figure S5 in SI). The molecular structure of the dinuclear complex **2** was illustrated in Figure 1-right**,** showing two uranyl units bridged via two μ_2-hydroxo groups with an overall U:bipy ratio of 1:1 in a single molecular unit. The coordination geometry around the U center in **2** is a distorted pentagonal bipyramidal polyhedron, which is similar to that in **1**. The dihedral angle between the N–U–N plane and the Cl–U–OH plane in **2** is 23.4°, which is significantly smaller than that in the mononuclear complex **1**. Consequently, the distortion of the uranyl equatorial plane in the dinuclear complex **2** is suppressed as compared with that in the mononuclear complex **1**. On the other hand, the bipy ligands in **2** show a higher torsion angle of 17.1° as compared with **1**. This torsion angle of bipy in **2** is also significantly higher than those found in similar hydroxo-bridged dinuclear uranyl complexes with bipy derivatives[57] (Table S1 in SI), indicating the geometrical flexibility of pure bipy molecules upon crystallization. Further increase in the U:bipy ratio to 1:3 also resulted in the mixture of **1** and **2**. Hence, the U:bipy ratio of 1:1 is the only achievable stoichiometry for U(VI)-

bipy complexes at least in the solid state under the current aqueous conditions. This also suggests that the 1:1 complex is likely to be the predominant form even in solution, regardless of the ligand concentration.

One would expect similar coordination behavior between bipy and phen, although this is not the case for the complexation with U(VI). When bipy was replaced with phen and the relevant U(VI) complex was prepared under the same condition applied to the synthesis of the complex **1**, the complex with a U:phen stoichiometry of 1:2 (i.e., $[UO_2(phen)_2Cl_2]$) was obtained,[26] despite the initial stoichiometry of 1:1. This complex shows one of the most significantly bent uranyl units ($\angle$O–U–O = 161.8(1)°) reported thus far.[58-59] When the U:phen ratio was increased to 1:2, a dinuclear complex of $[(UO_2(phen)Cl)_2(\mu_2\text{-}OH)_2]\cdot 2H_2O$ (**3**), the analog to the complex **2**, was obtained. As shown in Figure 2-top, the complex **3** is also sevenfold coordinated with a distorted pentagonal bipyramid polyhedron around each U center, which is comparable to those found in the complexes **1** and **2**. The dihedral angle between the N–U–N and the Cl–U–OH planes is 10.8°, which is much smaller than that in the analog complex of **2**. This originates primarily from the higher stiffness of phen molecules than that of bipy, which is also manifested in the observed smaller torsion angle ($\angle$N1–C5–C9–N2) of the phen molecule (4.11°). The torsion angle observed in the complex **3** is, however, the largest torsion angle for the phen molecule among the hydroxo-bridged dinuclear uranyl-phen complexes reported thus far (Table S1 in SI). In contrast to the bipy complex **2**, the crystal structure of **3** contains water molecules intercalated between the adjacent dinuclear uranyl molecules. These water molecules link the "*yl*"-oxygens to the adjacent bridging hydroxo groups via hydrogen bonding. This hydrogen bonding network is further extended along the [100] direction (Figure 2-top). Such intercalated water molecules are not observed in the crystal structure of the bipy compound **2**. This is presumably due to the difference in chemical nature between bipy and phen. That is, as demonstrated by the torsion

angles in the complexes **2** and **3**, bipy molecules can behave more flexibly upon crystallization to minimize voids in a unit cell than the phen ones. This is also substantiated by a smaller unit cell (V) with a higher density (ρ) for the complex **2** than those for the complex **3** (Table S3 in SI). Additionally, the rigid plane arrangement of phen molecules is known to facilitate the formation of π···π stacking interactions,[60] even in uranyl(VI)-phen complexes.[58] In fact, the Hirshfeld surface analysis[45-46] and the relevant 2D fingerprint plots[61] on the compound **3** reveal that there is a significant contribution of π···π interactions (12.5%) to the whole intermolecular interactions of the phen compound **3** (Figure 3-(a)). This limits the packing manner of the dinuclear uranyl-phen unit ([$(UO_2(phen)Cl)_2(\mu_2\text{-}OH)_2$]) upon crystallization, eventually creating additional spaces (voids) among the dinuclear uranyl-phen units (Figure 2-bottom), where water molecules can penetrate. Such a packing manner guided by π···π interactions is not significant in the crystallization of the bipy complex **2**, which is supported by a small contribution of π···π interactions (4.9%) in the compound **2** (Figure 3-(a)). All these facts indicate that, albeit their similarity in coordination manner toward metal cations including U(VI), bipy and phen behave differently upon crystallization.

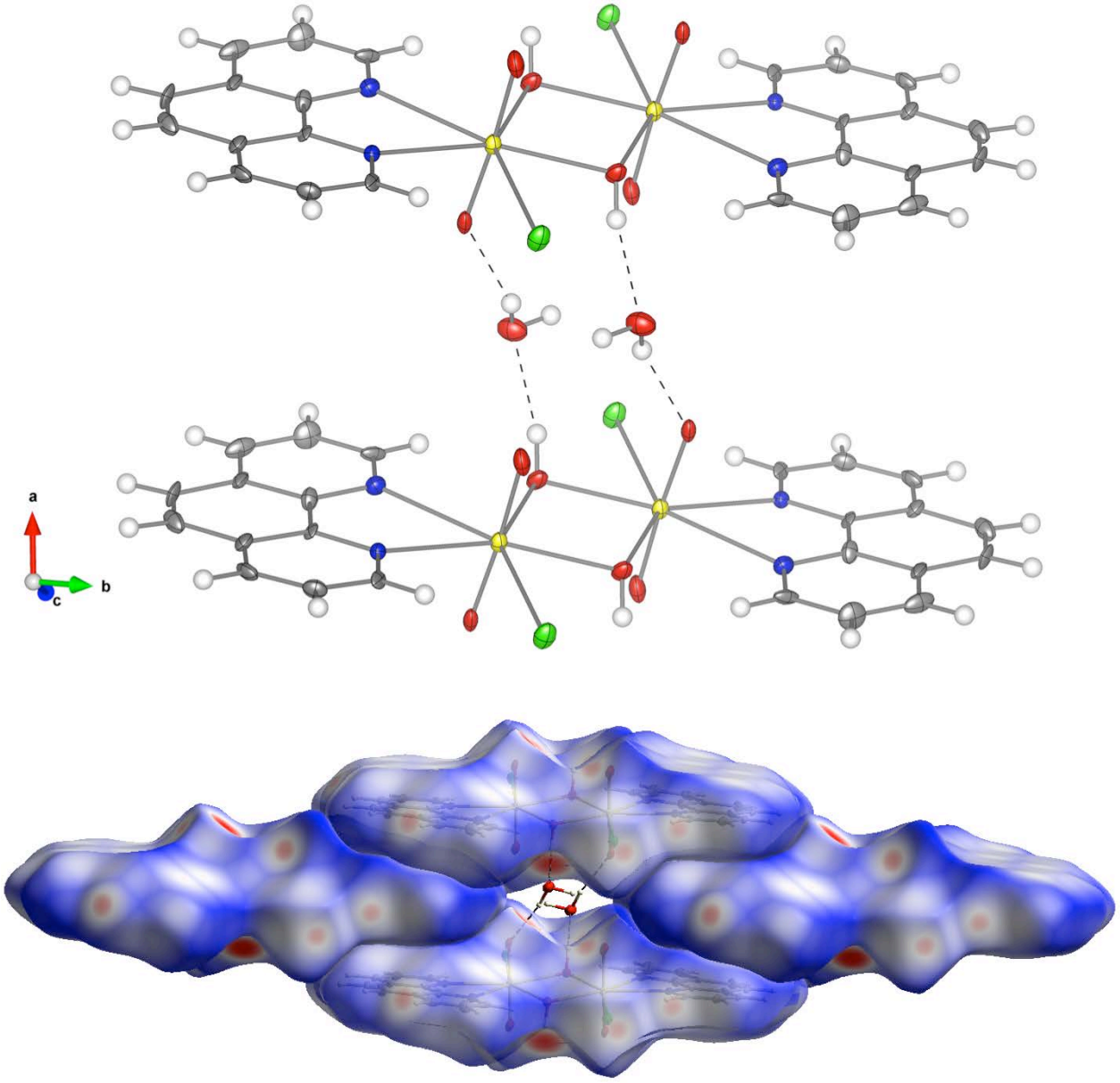

Figure 2. (Top) Molecular packing of $[(UO_2(phen)Cl)_2(\mu_2\text{-}OH)_2]\cdot 2H_2O$ (**3**) via hydrogen bonding network and (bottom) molecular packing of **3** along the [1−11] projection with the Hirshfeld surfaces mapped with d_{norm}[45] and hydrogen bonding network, showing a void to intercalate water molecules among the molecules. Thermal ellipsoids are drawn at 50% probability level. Color code: hydrogen (H, white), carbon (C, dark gray), chlorine (Cl, light green), nitrogen (N, blue), oxygen (O, red), and uranium (U as U^{6+}, yellow).

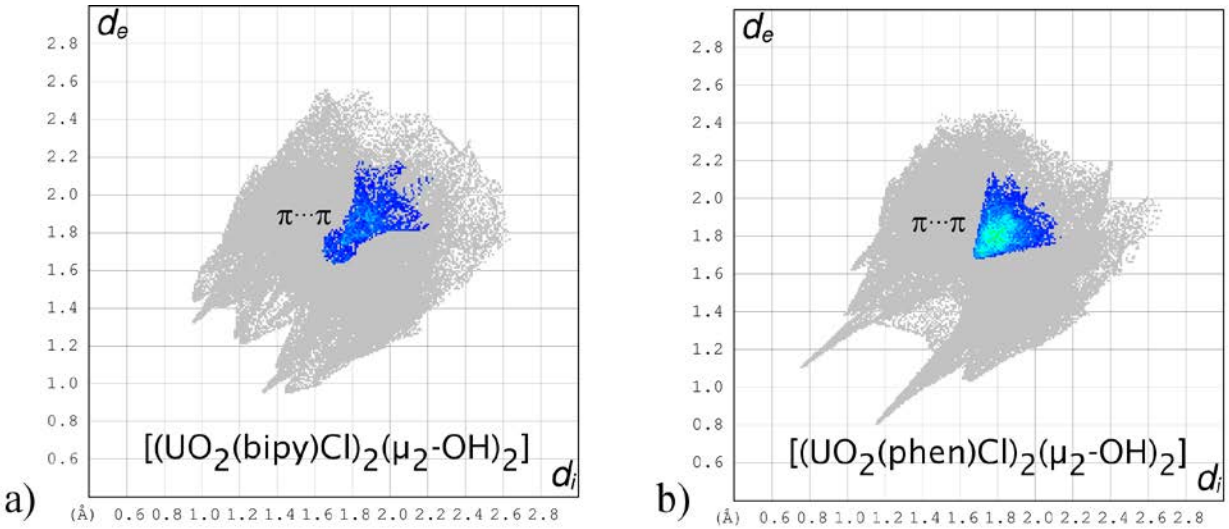

Figure 3. 2D fingerprint plots[61] for a) $[(UO_2(bipy)Cl)_2(\mu_2\text{-}OH)_2]$ and b) ($[(UO_2(phen)Cl)_2(\mu_2\text{-}OH)_2]$). The whole intermolecular interactions are shown in grey and direct π···π interactions are highlighted in blue-green, the color graduation of which represents the actual contribution of the interaction to the whole Hirshfeld surfaces (ranging from blue (little contributions) over green to red (high contribution)).

3.1.2. U(VI)-Fe(II) system

The combination of U(VI) and Fe(II) is of particular relevance to natural environmental systems, as Fe(II) is one of the major abiotic- and naturally occurring reductants even for uranium.[26, 62] The homogeneous redox reaction between U(VI) and Fe(II) in aqueous media is thermodynamically favored but kinetically restricted,[63] which makes the synthesis of hetero-metallic U(VI)/Fe(II) compounds possible. When mixing U(VI) with Fe(II) in the presence of bipy, a hetero-metallic compound of $[Fe(bipy)_3][UO_2Cl_4]$ (**4**) was obtained. The molecular arrangement of the compound **4** is shown in Figure 4-(a). When bipy was replaced with phen, the isostructural compound of $[Fe(phen)_3][UO_2Cl_4]$ (**5**) was synthesized. In these isostructural compounds, the iron is surrounded by three bidendate N-donor ligands, forming the well-known octahedral tris bipy/phen Fe(II) complexes. The uranium is present as the uranyl(VI) entity ($[UO_2]^{2+}$), which is coordinated by four chloride ions on the equatorial plane to form a square bipyramidal $[UO_2Cl_4]^{2-}$ complex, which is a common form of U(VI) in concentrated chloride systems.[64-67]

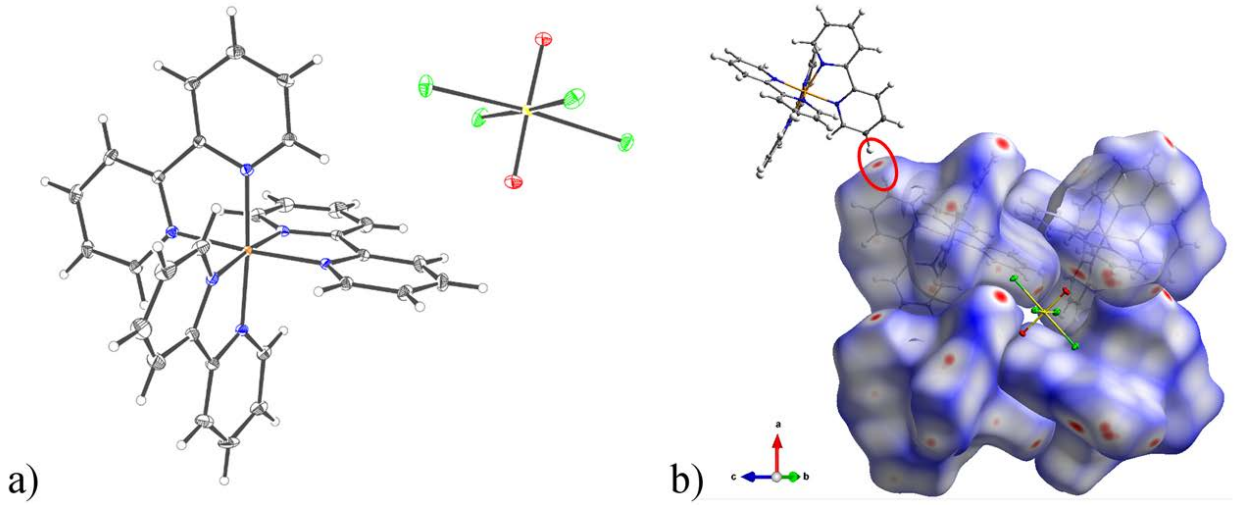

Figure 4. a) ORTEP plot of $[Fe(bipy)_3][UO_2Cl_4]$ (**4**) and b) molecular packing of **4** with the Hirshfeld surfaces mapped with d_{norm}. Thermal ellipsoids are drawn at 50% probability level. Color code: hydrogen (H, white), carbon

(C, dark gray), chlorine (Cl, light green), nitrogen (N, blue), oxygen (O, red), iron (Fe, orange), and uranium (U as U^{6+}, yellow).

Both the octahedral tris-bipy and -phen Fe(II) complexes exhibit chirality at the iron center. In fact, both the compounds **4** and **5** are crystallized as a racemic mixture, which is manifested by the determined centrosymmetric space group of $P2_1/c$. This indicates that no specific enantiomer is preferentially formed in the aqueous conditions applied in this study. The presence of enantiomers in the system also leads to another difference in crystal packing between the bipy and phen complexes, in addition to their difference in chemical nature (i.e. stiffness and π···π interactions). Albeit exhibiting the same space group of $P2_1/c$, the crystal structure (e.g. lattice parameters and volume (V)) of **4** and **5** significantly differs (Table S3 in the SI). Due to the higher flexibility of bipy than phen, the π···π interactions in the bipy compound **4** are less encouraged, resulting in the formation of edge-to-face π interactions, rather than the face-to-face π···π interactions, between the adjacent $[Fe(bipy)_3]^{2+}$ units (Figure 4-(b) and Figure S15 in SI). This leads to a one-dimensional network along the [001] direction with alternating the chirality of the $[Fe(bipy)_3]^{2+}$ units (Figure S15 in SI). Due to the alternation of chirality of the $[Fe(bipy)_3]^{2+}$ units, the one-dimensional network eventually forms a zigzag structure to make voids where the $[UO_2Cl_4]^{2-}$ units are well fitted. It seems that the energy gain from such a packing manner overcomes the repulsive and therefore less preferred H···H interactions between the adjacent $[Fe(bipy)_3]^{2+}$ units (the red spots highlighted with a circle in Figure 4-(b)). These close contacts of H···H interactions in the compound **4** are clearly visible as a sharp feature in the shorter d_i/d_e region[61] (highlighted with a red circle) in the 2D-fingerprint plot of the Hirshfeld surfaces of the $[Fe(bipy)_3]^{2+}$ unit (Figure 5-(a)). In contrast, such short contact H···H interactions are not observed in the phen compound **5** (highlighted with an orange circle in Figure 5-(c)), in which the intermolecular interactions are mainly dominated by direct π···π interactions between the adjacent $[Fe(phen)_3]^{2+}$ units. In the crystal structure of **5**, a pair of $[Fe(phen)_3]^{2+}$ enantiomers is connected

via face-to-face π-stacking interactions (Figure S16 in SI). This π-stacking network is, however, not extended in any directions, which is in contrast to the monometallic uranyl(VI) phen compound **3**. This is presumably due to the steric restrictions caused by the bulkiness of the $[Fe(phen)_3]^{2+}$ units. The lack of extensive π-stacking networks upon the crystal packing of **5** alternatively results in the formation of hydrogen bonding between the aromatic hydrogen of phen and the "*yl*" oxygen of the $[UO_2Cl_4]^{2-}$ units (Figures S16 and S17 in SI). The formation of such hydrogen bonding is also obvious in the 2D-fingerprint plot for the $[UO_2Cl_4]^{2-}$ unit in **5** (Figure 5-(d)), where a sharp feature is observed in the shorter d_i/d_e region (highlighted with a green circle). In contrast, no such hydrogen bonding is observed in **4**, which is illustrated by the absence of sharp feature in the 2D-fingerprint plot for the $[UO_2Cl_4]^{2-}$ unit in **4** (blue circle in Figure 5-(b)).

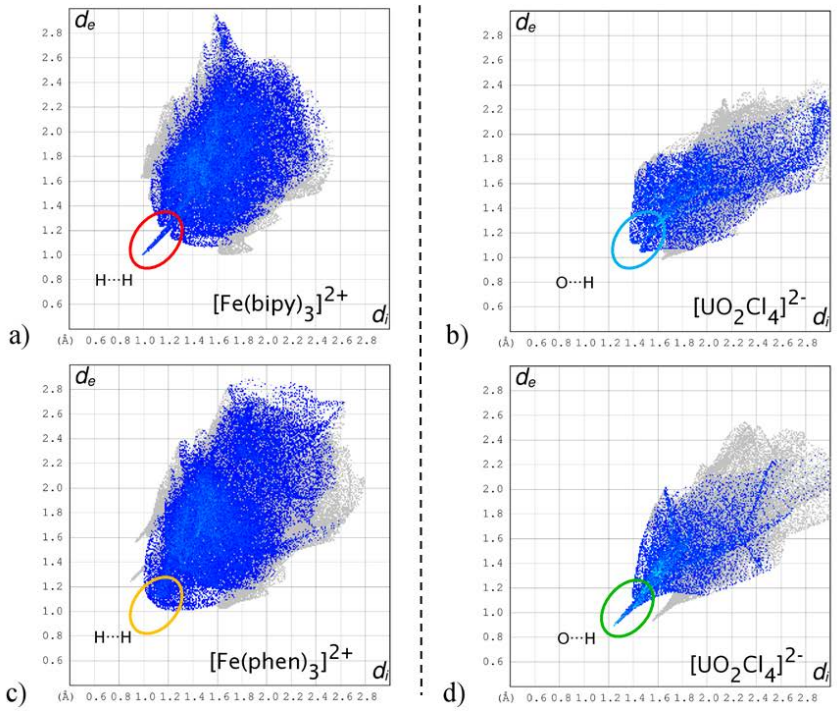

Figure 5. 2D fingerprint plots for $[Fe(bipy)_3][UO_2Cl_4]$ (**4**); plots for the $[Fe(bipy)_3]^{2+}$ (a) and $[UO_2Cl_4]^{2-}$ units (b), and the plots for $[Fe(phen)_3][UO_2Cl_4]$ (**5**); plots for the $[Fe(phen)_3]^{2+}$ (c) and $[UO_2Cl_4]^{2-}$ units (d). Only H···H and O···H interactions are displayed with colors in the plots of $[Fe(bipy/phen)_3]^{2+}$ and $[UO_2Cl_4]^{2-}$, respectively. The color in the plots depicts the actual contribution of each interaction to the whole Hirshfeld surfaces, ranging from blue (little contributions) over green to red (high contribution). The interactions of main interest in the text (i.e. short contact

interactions) are highlighted with circles. Interactions other than H···H (a and c) and O···H (b and d) interactions are shown in grey.

3.1.3. U(VI)-Fe(III) system

Due to their dominant presence in the natural environment which is mostly an oxidizing atmosphere, the combination of U(VI) and Fe(III) is the most relevant to the possible interactions of these two metals under environmental conditions. The interaction of U(VI) (as UO_2^{2+}) and Fe(III) in an aqueous solution in the presence of bipy or phen resulted in the formation of isostructural compounds, $[(Fe(bipy)_2Cl)_2(\mu_2\text{-}O)][UO_2Cl_4]\cdot H_2O$ (**6**) and $[(Fe(phen)_2Cl)_2(\mu_2\text{-}O)][UO_2Cl_4]$ (**7**), respectively. As also observed in the compounds **4** and **5**, the uranium in **6** and **7** exists as the anionic $[UO_2Cl_4]^{2-}$ unit, while the iron (as Fe(III)) is forming a cationic oxo-bridged dinuclear complex of $[(Fe(L)_2Cl)_2(\mu_2\text{-}O)]^{2+}$ (L = bipy or phen), instead of the mononuclear tris bipy/phen complex observed in **4** and **5**. In this cationic dinuclear complex, each Fe center is surrounded by two bidendate N-donor ligands, one Cl and one bridging O atom connecting the two Fe centers, forming a distorted octahedron around the Fe center. The two Fe atoms and bridging O atom are not linearly arranged in the compounds **6** and **7**, but with the Fe–O–Fe angle of 163.5(2)° and 168.2(4)°, respectively. These angles are comparable to those in the reported μ_2-oxo-bridged dinuclear iron(III) complexes.[68-69] The cationic $[(Fe(L)_2Cl)_2(\mu_2\text{-}O)]^{2+}$ unit is further stabilized via intramolecular hydrogen bonds C1–H1···Cl3 (Figure 6) and intramolecular π-stacking effects (Figures S18 and S19 in SI). Furthermore, the cationic Fe units in both compounds **6** and **7** show chirality around the Fe center, resulting in the formation a racemic mixture with the same centrosymmetric space group of C2/c upon crystallization. The lattice parameters of the compounds **6** and **7** are well comparable to each other, which is in contrast to the difference observed between the U(VI)-Fe(II) compounds **4** and **5**.

Due to the flexibility of bipy molecules, the crystal packing of **6** results in the formation of only a single type of π-stacking network (Figure S18 in SI), while the compound **7** with more rigid phen

molecules involves there different types of π-stacking networks (Figure S19 in SI). These enhanced π···π interactions between the adjacent phen molecules in **7** lead to denser crystal packing, eventually showing a higher density (ρ) of **7** than that of **6**, despite a larger unit cell volume (V) for **7** than that for **6** (Table S3 in SI). This trend observed between the bipy compound **6** and the phen one **7** is in contrast to those observed between the previous bipy and phen compounds of **2** and **3**, and **4** and **5**. The less dense packing of the bipy compound **6** also produces voids in the crystal structure, where water molecules can be incorporated (one water molecules per formula unit). These water molecules are populated at several crystallographic positions, connecting the cationic $[(Fe(bipy)_2Cl)_2(\mu_2\text{-}O)]^{2+}$ units via hydrogen bonds (Figure 6-(a)). On the other hand, the denser packing of the phen compound **7** produces no voids where water molecules can penetrate and, hence, no water molecules are incorporated in the crystal structure of **7**.

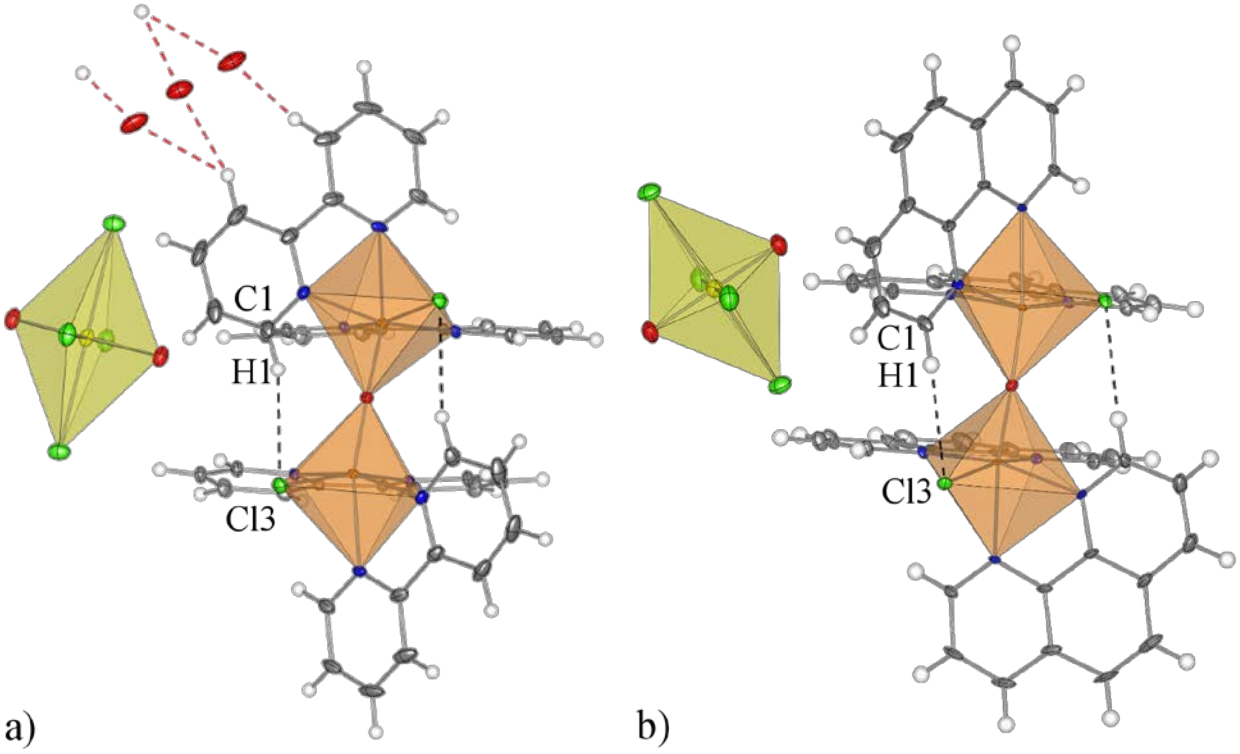

Figure 6. a) Molecular structure of $[(Fe(bipy)_2Cl)_2(\mu_2\text{-}O)][UO_2Cl_4]\cdot H_2O$ (**6**) and b) $[(Fe(phen)_2Cl)_2(\mu_2\text{-}O)][UO_2Cl_4]$ (**7**). Thermal ellipsoids are drawn at 50% probability level. Intra- and intermolecular hydrogen bonds are illustrated with black- and red dash lines, respectively. Color code: hydrogen (H, white), carbon (C, dark gray), chlorine (Cl, light green), nitrogen (N, blue), oxygen (O, red), iron (Fe, orange), and uranium (U as U^{6+}, yellow).

The hydrogen bonds $H\cdots O_w$ in **6** (red dash lines in Figure 6-(a)) are also visible in the 2D fingerprint plot of the Hirshfeld surfaces for the cationic $[(Fe(bipy)_2Cl)_2(\mu_2\text{-}O)]^{2+}$ unit in **6** (Figure 7-(a)). The contribution of $H\cdots O$ interactions to the overall intermolecular interactions for the $[(Fe(bipy)_2Cl)_2(\mu_2\text{-}O)]^{2+}$ unit is close to 15%, whereas the contribution of $H\cdots O$ is negligible (4%) for the $[(Fe(phen)_2Cl)_2(\mu_2\text{-}O)]^{2+}$ unit in **7**.

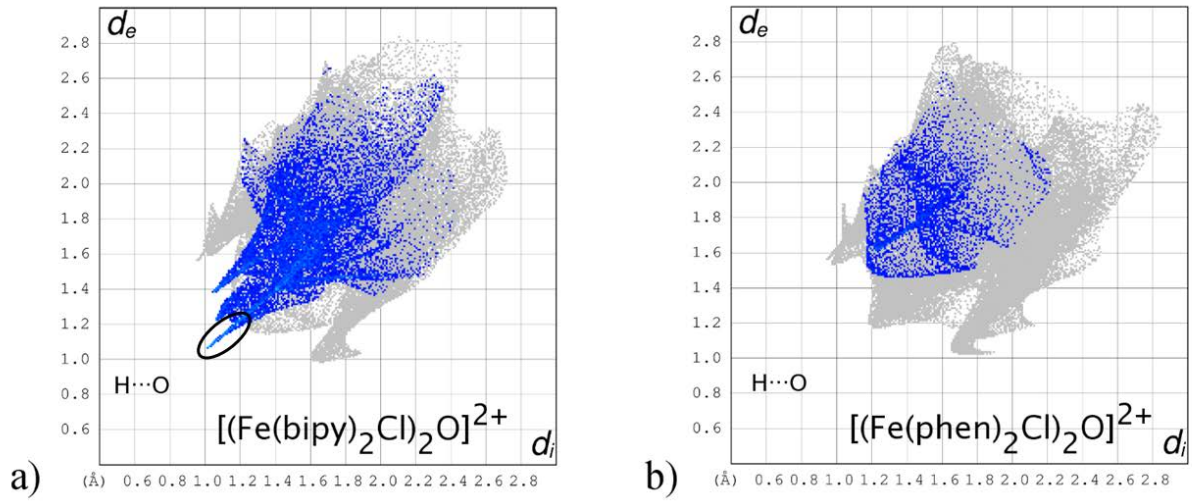

Figure 7. 2D fingerprint plots for $[(Fe(L)_2Cl)_2(\mu_2\text{-}O)]^{2+}$ units of $[(Fe(bipy)_2Cl)_2(\mu_2\text{-}O)][UO_2Cl_4]\cdot H_2O$ (**6**) (a) and $[(Fe(phen)_2Cl)_2(\mu_2\text{-}O)][UO_2Cl_4]$ (**7**) (b). Only H···O interactions are displayed with colors. The color in the plots depicts the actual contribution of the interaction to the whole Hirshfeld surfaces, ranging from blue (little contributions) over green to red (high contribution). The $H\cdots O_w$ interactions with the incorporated water molecules in **6** are highlighted with a circle. Interactions other than H···O interactions are shown in grey.

The difference observed for the cationic $[(Fe(bipy)_2Cl)_2(\mu_2\text{-}O)]^{2+}$ and $[(Fe(phen)_2Cl)_2(\mu_2\text{-}O)]^{2+}$ units can be further attributed to the different arrangement of the anionic counterparts of $[UO_2Cl_4]^{2-}$ units. Hence, the contribution of H···O interactions to the overall Hirshfeld surfaces of the $[UO_2Cl_4]^{2-}$ unit is more significant in the bipy compound **6** than the phen compound **7** (Figure S20 in SI).

Regardless of the oxidation state of Fe, the resultant U(VI)-Fe compounds **4**-**8** are always composed of the anionic U(VI)-Cl unit (i.e. $[UO_2Cl_4]^{2-}$) and the cationic Fe-bipy/phen unit ($[Fe(L)_3]^{2+}$ or $[(Fe(L)_2Cl)_2(\mu_2\text{-}O)]^{2+}$). This indicates that the diamine ligands interact more preferentially with Fe ions than with U(VI), while Cl anions are attracted more strongly to U(IV) than to Fe ions under the current aqueous condition.

3.2. Tetravalent uranium (U(IV))

In contrast to the linear uranyl(VI) cation, the tetravalent uranium (U(IV)) exists as a highly charged spherical U^{4+} cation in solution.[70-71] Due to its high charge density, U(IV) exhibits a strong hydrolysis tendency, forming hydrolysis products even under the acidic condition.[72] As a counterpart of the previous section 3.1, this section focuses on the investigation into the interaction of U(IV) with Fe ions in the presence of the diamine ligands in an aqueous solution.

3.2.1. Pure U(IV)-Ligand system

Similarly to the previous section **3.1**, the pure interaction between U(IV) and bipy/phen was investigated in an aqueous solution prior to the hetero-metallic U(IV)-Fe system. When a stoichiometric amount of U(IV) and bipy/phen are reacted in a water/acetone mixture, the two compounds, $[Hbipy]_2[UCl_6]$ (**8**) and $[Hphen]_2[UCl_6]$ (**9**), were obtained as a pure phase. These compounds have already been reported by Gans *et al.*,[73] but not yet been structurally described. Their molecular structures characterized in this study are shown in Figure 8.

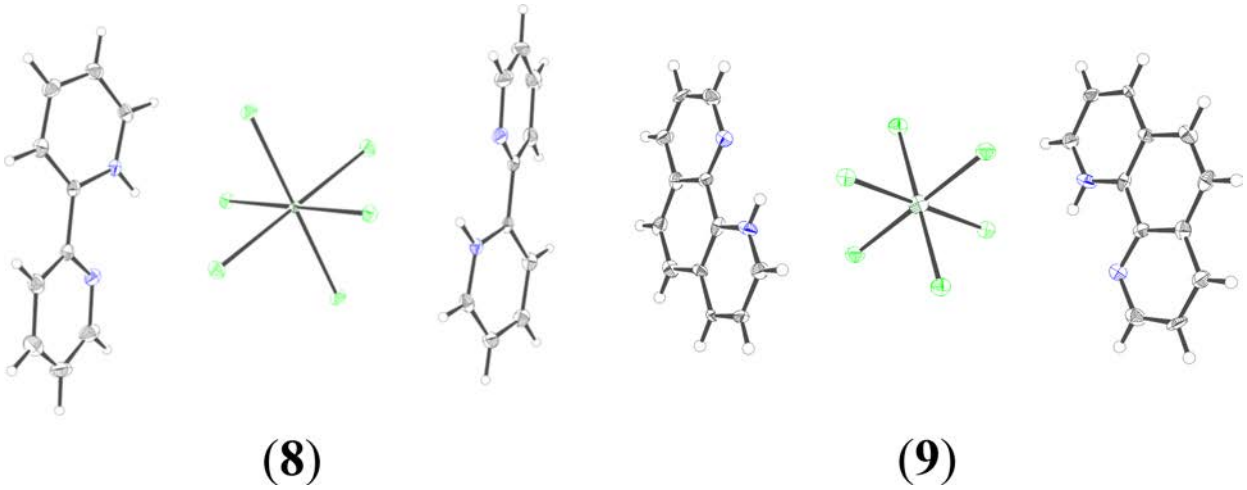

Figure 8. ORTEP plots of $[Hbipy]_2[UCl_6]$ (**8**, left) and $[Hphen]_2[UCl_6]$ (**9**, right). Thermal ellipsoids are drawn at 50% probability level. Color code: hydrogen (H, white), carbon (C, dark gray), chlorine (Cl, light green), nitrogen (N, blue), and uranium (U as U^{4+}, dark green).

The U(IV) in both **8** and **9** is coordinated by six chloride anions to form octahedral $[UCl_6]^{2-}$ anionic unit. The average U–Cl distances in **8** and **9** (Table 1) are consistent with those of the $[UCl_6]^{2-}$ units formed in the presence of other organic cations such as pyridinium[74], ammonium[75] or phosphonium[76] derivatives. One of the pyridine groups of the bipy/phen molecules in **8** and **9** is protonated to form $[Hbipy]^+$ and $[Hphen]^+$ cations, respectively. The $[Hbipy]^+$ unit in **8** shows a *cis* geometry in terms of the position of N atoms. Albeit both compounds are crystallized in the same triclinic space group *P-1*, there is a significant difference in their lattice parameters (Table S3 in SI), suggesting a different manner of intermolecular interactions between **8** and **9**. This is also manifested by the differences in crystal density (ρ) and cell volume (V) between these compounds. In the compound **8**, the adjacent two $[UCl_6]^{2-}$ units are linked by the hydrogen bonds *via* two $[Hbipy]^+$ units to form a one-dimensional hydrogen bond network along the [-11-1] direction (Figure S21 in SI). In contrast, the crystal packing of the compound **9** leads to the formation of an intermolecular π-stacking network between the adjacent phen molecules (Figure S22 in SI), which eventually results in the higher crystal density (i.e. denser crystal packing) of **9** than that of **8**. The enhanced π···π interactions in **9** are also clearly visible in the 2D fingerprint plots of the Hirshfeld surfaces of **8** and **9** (Figure 9). The overall contribution of π···π interactions in the bipy compound **8** is negligible (4.0%), while the contribution in the phen compound **9** is significant (14.4%). In contrast to this difference in Hirshfeld surfaces between the cationic organic units in **8** and **9**, the Hirshfeld surfaces of their anionic counterparts of $[UCl_6]^{2-}$ units show no significant difference (Figure S23 in SI).

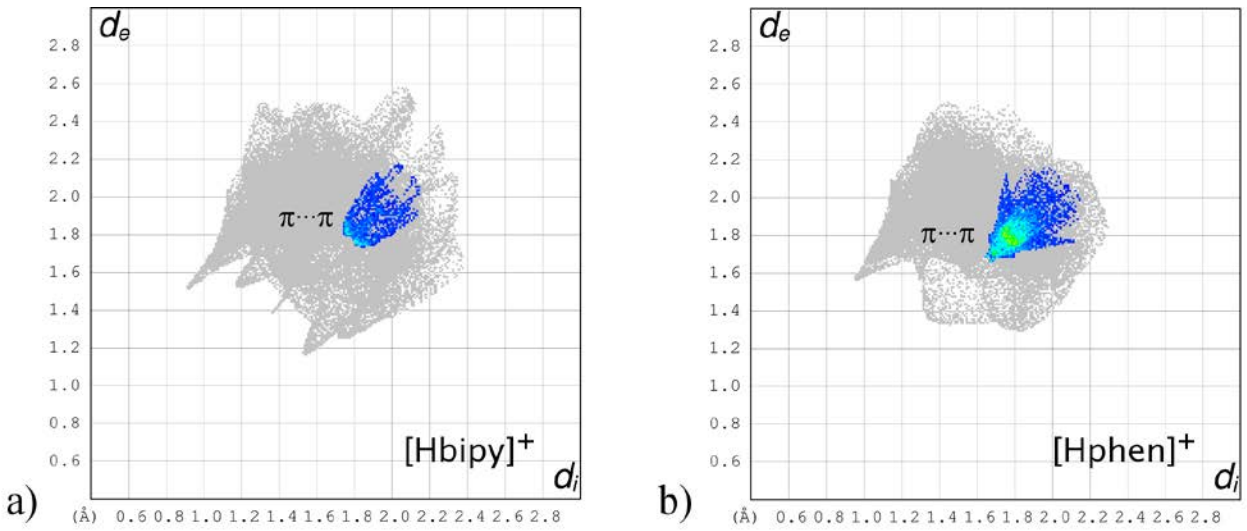

Figure 9. 2D fingerprint plots[61] for the $[Hbipy]^+$ unit of $[Hbipy]_2[UCl_6]$ (**8**) (a) and the $[Hphen]^+$ unit of $[Hphen]_2[UCl_6]$ (**9**) (b). The whole intermolecular interactions are shown in grey and direct π···π interactions are highlighted with colors, the color graduation of which represents the actual contribution of the interaction to the whole Hirshfeld surfaces (ranging from blue (little contributions) over green to red (high contribution)).

When increasing the U:ligand ratio to 1:2 or 1:3, dark blue/green precipitate was formed. The PXRD profile of the resultant precipitate reveals the formation of nanocrystalline UO_2 (Figure S14 in SI). It is well known that the strong hydrolysis tendency of U(IV) induces the formation of UO_2 (or $UO_2(H_2O)_n$) even under acidic conditions.[77] As a matter of fact, due to the protonation ability of the diamine ligands, an increase in the ligand concentration rises the pH value of the sample solution (Table S2 in SI), enhancing the hydrolysis of U(IV) to eventually form UO_2. The hydrolysis of U(IV) can also produce an additional source of Cl^- to form the $[UCl_6]^{2-}$ unit from the initial compound of UCl_4 (Section 4 in SI). All these results indicate that the coordination of the diamine ligands towards U(IV) is not strong enough to form coordinative compounds at least in the aqueous conditions applied in this study.

3.2.2. U(IV)-Fe(II) system

U(IV) and Fe(II) are supposed to coexist under reducing conditions. As discussed in the previous subsection 3.2.1, the pure interaction between U(IV) and bipy/phen with a larger than a stoichiometric amount results in the formation of UO_2 as a precipitate. However, when Fe(II) was added into this system under the same aqueous condition, no precipitation occurs. Further evaporation of the mixed U(IV)-Fe(II)-ligand solution in vacuo yielded two isostructural compounds of $[Fe(bipy)_3][UCl_6]$ (**10)** and $[Fe(phen)_3][UCl_6]$ (**11**). As a representative, the molecular structure of **10** is shown in Figure 10-(a). Both compounds **10** and **11** consist of the already known cationic unit of Fe(II) (i.e. $[Fe(L)_3]^{2+}$ unit; L = bipy or phen) and anionic unit of U(IV) (i.e. $[UCl_6]^{2-}$ unit), although its combination as a single compound is reported in this study for the first time. The Fe–N distances in the cationic $[Fe(L)_3]^{2+}$ units (L = bipy or phen) are in good agreement with those found in the previous U(VI)-Fe(II) compounds of **4** and **5**, showing the same trend of bond lengthening originating from the higher stiffness of phen than that of bipy (Table 1). The average U–Cl distances in the $[UCl_6]^{2-}$ units in **10** and **11** are also well comparable with those in the mono-metallic U(IV) compounds of **8** and **9** (Table 1).

Table 1. Summary of selected bond distances in the compounds **4-7**

	4: U(VI)-Fe(II)-bipy	**5: U(VI)-Fe(II)-phen**	**6: U(VI)-Fe(III)-bipy**	**7: U(VI)-Fe(III)-phen**
d(U–O_{yl}) [Å]	1.768(1)	1.772(2)	1.775(2)	1.761(5)
d(U–Cl) [Å]	2.680(1)	2.661(1)	2.683(1)	2.667(2)
d(Fe–N) [Å]	1.964(1)	1.977(3)	2.178(3)	2.191(5)
	8: U(IV)-bipy	**9: U(IV)-phen**	**10: U(IV)-Fe(II)-bipy**	**11: U(IV)-Fe(II)-phen**
d(U–Cl) [Å]	2.625(1)	2.616(1)	2.623(1)	2.61(1)
d(Fe–N) [Å]	-	-	1.968(1)	1.97(3)

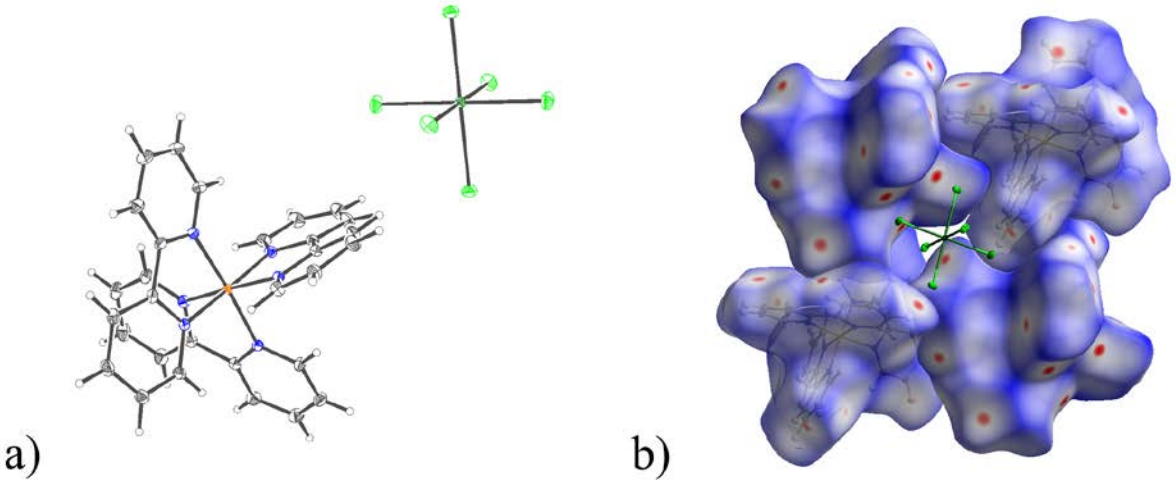

Figure 10. a) ORTEP plot of $[Fe(bipy)_3][UCl_6]$ (**10**), and b) molecular packing of **10** with the Hirshfeld surfaces mapped with d_{norm}. Thermal ellipsoids are drawn at 50% probability level. Color code: hydrogen (H, white), carbon (C, dark gray), chlorine (Cl, light green), nitrogen (N, blue), iron (Fe, orange), and uranium (U as U^{4+}, dark green).

The intermolecular interactions in $[Fe(bipy)_3][UCl_6]$ (**10**) are illustrated in Figure 10-(b), showing the molecular packing of a single anionic $[UCl_6]^{2-}$ unit surrounded with four cationic $[Fe(bipy)_3]^{2+}$ units. This clearly indicates significant H···Cl hydrogen bonds between the $[UCl_6]^{2-}$ unit and the adjacent bipy ligands (highlighted as red spots on the Hirshfeld surface in Figure 10-(b)), which is also manifested in the 2D fingerprint plots of **10** (Figure S25 in SI). Due to the flexibility of the bipy ligand, no π···π interactions between the adjacent $[Fe(bipy)_3]^{2+}$ units are formed in the crystal packing of **10**. Instead, the molecular packing of **10** is composed mainly of the H···Cl hydrogen bonds around the $[UCl_6]^{2-}$ unit. In fact, the $[Fe(bipy)_3]^{2+}$ and $[UCl_6]^{2-}$ units in **10** are linearly placed along the [001] direction in the rhombohedral unit cell to form columnar structures (Figure S24 in SI). In contrast to the bipy compound **10**, the phen compound **11** shows a completely different packing manner by forming the inter-unit interactions between the adjacent enantiomeric $[Fe(phen)_3]^{2+}$ units via face-to-face π···π interactions (Figure S26 in SI) that are identical to those observed in the U(VI)-Fe(II)-phen compound **5**. The crystal density (ρ) and cell

volume (V) for the bipy compound **10** is larger than those for the phen compound **11**, which is the same trend observed for the analogous U(VI) compounds **4** and **5** (Table 3 in SI**)**. The improved symmetry (O_h) of the [UCl_6^{2-}] unit as compared with the D_{4h} symmetry for the [$UO_2Cl_4^{2-}$] unit eventually introduces a three-fold rotation axis, whereas the compound **10** crystallizes in the rhombohedral space group $R\bar{3}$. This is not observed for the corresponding U(VI) compound **4**.

3.2.3. U(IV)-Fe(III) system

The last possible combination of U(IV) and Fe(III) was examined by mixing UCl_4 and $FeCl_3$ in an aqueous solution. However, the interaction of reducing U(IV) and oxidizing Fe(III) resulted in the expected redox reaction to eventually form U(VI) and Fe(II). Despite many attempts under different conditions to obtain U(IV)-Fe(III) compounds, no hetero-metallic U(IV)-Fe(III) compounds could be obtained at least under the conditions applied in this study.

4. CONCLUSION

A systematic study on the complexation behavior of iron and uranium in the presence of the bidendate *N*-donor ligand, 2,2'-bipyridine (bipy) or 1,10-phenanthroline (phen), was performed in an aqueous solution to cover all the combinations of possible redox couples (i.e. Fe^{2+}/Fe^{3+} and U^{4+}/U^{6+}) and U(IV/VI)). In addition to three U compounds with bipy/phen (**1**-**3**), six new hetero-metallic Fe-U compounds, ($[Fe^{II}(bipy)_3][U^{VI}O_2Cl_4]$ (**4**), $[Fe^{II}(phen)_3][U^{VI}O_2Cl_4]$ (**5**), $[(Fe^{III}(bipy)_2Cl)_2(\mu_2\text{-}O)][U^{VI}O_2Cl_4]\cdot H_2O$ (**6**), $[(Fe^{III}(phen)_2Cl)_2(\mu_2\text{-}O)][U^{VI}O_2Cl_4]$ (**7**), $[Fe^{II}(bipy)_3][U^{IV}Cl_6]$ (**10**), $[Fe^{II}(phen)_3][U^{IV}Cl_6]$ (**11**), were successfully synthesized and characterized in solid state. A comparison between the pure U complexes and the hetero-metallic Fe-U complexes revealed that, regardless of the oxidation states of Fe and U, both diamine ligands interacts more preferentially with iron than uranium in the aqueous conditions applied in this study, forming a mononuclear $[FeL_3]^{2+}$ unit and a dinuclear μ_2-oxo-bridged $[(FeL_2Cl)_2(\mu_2\text{-}O)]^{2+}$ unit (L = bipy or phen) for Fe(II) and –(III), respectively. On the other hand, uranium interacts with chloride anions to form anionic $[UCl_6]^{2-}$ and $[UO_2Cl_4]^{2-}$ units for U(IV) and –(VI), respectively. The observed trend can be explained by the higher Lewis acidity of U cations than that of Fe cations. Hence, Fe cations are expected to interact more preferably with moderately hard (or soft) donor atoms, such as nitrogen, than U cations.

In the absence of iron, U(VI) can interact with both diamine ligands in an aqueous solution to form coordinative compounds. The manner of crystal packing of the obtained compounds is, however, significantly different between the bipy- and phen compounds. The observed difference stems from the higher stiffness of the phen ligand than the bipy ligand. That is, upon crystallization, the stiffer phen ligand tends to enhance direct $\pi\cdots\pi$ interactions which are less

pronounced upon the formation of the bipy compound. This also applies to the formation of hetero-metallic Fe-U compounds.

The results obtained in this study indicate that, regardless of the oxidation states of the metals, the fundamental coordination properties of bipy/phen towards iron and/or uranium are well comparable, whereas their actual behavior upon crystallization is remarkably different. This could eventually lead to physical/chemical difference between the bipy- and phen compounds as a bulk material. Another important finding of this study is that, regardless of the combination of redox couple, both Fe and U cations always form ionic units (i.e. cationic Fe units and anionic U units) in the presence of the diamine ligands and chloride anions. This suggests that both Fe and U can form stable solution species in aqueous systems in the presence of bipy or phen, which would have potential implication particularly for the reliable assessment of the migration behavior of these metals under geological conditions relevant to mining or nuclear waste repositories.

ASSOCIATED CONTENT

The Supporting Information is available free of charge on the ACS Publications website at DOI: 10.1021/acs.inorgchem.

Powder-XRD profiles, TG-DSC data, molecular- and crystal structures not shown in the main text, 2D fingerprint plots of Hirshfeld surfaces that are not shown in the main text, a list of crystallographic data for the compounds **1**-**11**.

AUTHOR INFORMATION

Corresponding author

*E-mail: a.ikeda@hzdr.de

ORCID

Sebastian Schöne: 0000-0002-0723-7778, Atsushi Ikeda-Ohno: 0000-0003-3380-5211

Funding

This research work was funded by the German Federal Ministry of Education and Research (BMBF) under the project number 01176176/1 (FENABIUM). Part of the work was also conducted under the Reimei Research Program 2018, Japan Atomic Energy Agency.

Notes

The authors declare no competing financial interest.

REFERENCES

(1) Schubert, U. S.; Eschbaumer, C. Macromolecules Containing Bipyridine and Terpyridine Metal Complexes: Towards Metallosupramolecular Polymers. *Angew. Chem. Int. Ed.* **2002,** *41*, 2892-2926.

(2) Saha, M. L.; Neogi, S.; Schmittel, M. Dynamic heteroleptic metal-phenanthroline complexes: from structure to function. *Dalton Trans.* **2014,** *43*, 3815-3834.

(3) Ye, B.-H.; Tong, M.-L.; Chen, X.-M. Metal-organic molecular architectures with 2,2′-bipyridyl-like and carboxylate ligands. *Coord. Chem. Rev.* **2005,** *249*, 545-565.

(4) Wu, Y. Design and construction of diverse structures of coordination polymers: Photocatalytic properties. *J. Solid State Chem.* **2017,** *245*, 213-218.

(5) Roy, B. C.; Chakrabarti, K.; Shee, S.; Paul, S.; Kundu, S. Bifunctional Ru(II) - Complex - Catalysed Tandem C−C Bond Formation: Efficient and Atom Economical Strategy for the Utilisation of Alcohols as Alkylating Agents. *Chem. Eur. J.* **2016,** *22*, 18147-18155.

(6) Malkov, A. V.; Kocovsky, P. Chiral Bipyridine Derivatives in Asymmetric Catalysis. *Curr. Org. Chem.* **2003,** *7*, 1737-1757.

(7) Le Bozec, H.; Guerchais, V. Photochromic bipyridyl metal complexes: Photoregulation of the nonlinear optical and/or luminescent properties. *C. R. Chim.* **2013,** *16*, 1172-1182.

(8) Happ, B.; Winter, A.; Hager, M. D.; Schubert, U. S. Photogenerated avenues in macromolecules containing Re(I), Ru(II), Os(II), and Ir(III) metal complexes of pyridine-based ligands. *Chem. Soc. Rev.* **2012,** *41*, 2222-2255.

(9) Adelaide, M.; James, O. O. Antimicrobial, DNA cleavage and antitumoral properties of some transition metal complexes of 1,10 -phenanthroline and 2,2'-bipyridine: a review. *Elixir Appl. Chem.* **2014,** *67*, 21413-21420.

(10) Barton, J. K. Metals and DNA: molecular left-handed complements. *Science* **1986,** *233*, 727-734.

(11) Nielsen, P. E. Chemical and photochemical probing of DNA complexes. *J. Mol. Recognit.* **1990,** *3*, 1-25.

(12) Valensin, D.; Gabbiani, C.; Messori, L. Metal compounds as inhibitors of β-amyloid aggregation. Perspectives for an innovative metallotherapeutics on Alzheimer's disease. *Coord. Chem. Rev.* **2012,** *256*, 2357-2366.

(13) Sammes, P. G.; Yahioglu, G. 1,10-Phenanthroline: a versatile ligand. *Chemi. Soc. Rev.* **1994,** *23*, 327-334.

(14) Constable, E. C., Homoleptic Complexes of 2,2'-Bipyridine. In *Adv. Inorg. Chem.*, Sykes, A. G., Ed. Academic Press: 1989; Vol. 34, pp 1-63.

(15) McBryde, W. A. E., A critical review on equilibrium data for proton- and metal complexes of 1,10-Phenanthroline, 2,2'-Bipyridine and related compounds. In *IUPAC Chemical Data Series: Critical evaluation of equilibrium constants in solution, A: Stability constants of metal complexes* McBryde, W. A. E., Ed. 1978; Vol. 17.

(16) Blau, F. Über neue organische Metallverbindungen. *Monatsh. Chem.* **1898,** *19*, 647-689.

(17) Blau, F. Über die trockene Destillation von pyridincarbonsauren Salzen. *Monatsh. Chem.* **1889,** *10*, 375-388.

(18) Danon, J. J.; Krüger, A.; Leigh, D. A.; Lemonnier, J.-F.; Stephens, A. J.; Vitorica-Yrezabal, I. J.; Woltering, S. L. Braiding a molecular knot with eight crossings. *Science* **2017,** *355*, 159-162.

(19) Auboeck, G.; Chergui, M. Sub-50-fs photoinduced spin crossover in $[Fe(bpy)_3]^{2+}$. *Nature Comm.* **2015,** *7*, 629-633.

(20) Bousseksou, A.; Molnar, G.; Salmon, L.; Nicolazzi, W. Molecular spin crossover phenomenon: recent achievements and prospects. *Chem. Soc. Rev.* **2011,** *40*, 3313-3335.
(21) Hulanicki, A.; Glab, S., Indicator Characteristics In *Redox Indicators. Characteristics and Applications*, Pergamon: 1978; pp 473-497.
(22) Vanýsek, P., Electrochemical Series. In *CRC Handbook of Chemistry and Physics*, Lide, D. R., Ed. CRC Press/Taylor and Francis: Boca Raton, FL, 2010; Vol. 90.
(23) Naim, A.; Bouhadja, Y.; Cortijo, M.; Duverger-Nédellec, E.; Flack, H. D.; Freysz, E.; Guionneau, P.; Iazzolino, A.; Ould Hamouda, A.; Rosa, P.; Stefańczyk, O.; Valentín-Pérez, Á.; Zeggar, M. Design and Study of Structural Linear and Nonlinear Optical Properties of Chiral [Fe(phen)3]2+ Complexes. *Inorganic Chemistry* **2018**.
(24) Stewart, B. D.; Amos, R. T.; Nico, P. S.; Fendorf, S. Influence of Uranyl Speciation and Iron Oxides on Uranium Biogeochemical Redox Reactions. *Geomicrobiol. J.* **2011,** *28*, 444-456.
(25) Latta, D. E.; Gorski, C. A.; Boyanov, M. I.; O'Loughlin, E. J.; Kemner, K. M.; Scherer, M. M. Influence of Magnetite Stoichiometry on U(VI) Reduction. *Environ. Sci. Technol.* **2012,** *46*, 778-786.
(26) O'Loughlin, E. J.; Kelly, S. D.; Cook, R. E.; Csencsits, R.; Kemner, K. M. Reduction of Uranium(VI) by Mixed Iron(II)/Iron(III) Hydroxide (Green Rust): Formation of UO2 Nanoparticles. *Environ. Sci. Technol.* **2003,** *37*, 721-727.
(27) Crane, R. A.; Dickinson, M.; Popescu, I. C.; Scott, T. B. Magnetite and zero-valent iron nanoparticles for the remediation of uranium contaminated environmental water. *Water Res.* **2011,** *45*, 2931-2942.
(28) Yan, S.; Hua, B.; Bao, Z.; Yang, J.; Liu, C.; Deng, B. Uranium(VI) Removal by Nanoscale Zerovalent Iron in Anoxic Batch Systems. *Environ. Sci. Technol.* **2010,** *44*, 7783-7789.
(29) Fiedor, J. N.; Bostick, W. D.; Jarabek, R. J.; Farrell, J. Understanding the Mechanism of Uranium Removal from Groundwater by Zero-Valent Iron Using X-ray Photoelectron Spectroscopy. *Environ. Sci. Technol.* **1998,** *32*, 1466-1473.
(30) Yan, S.; Chen, Y.; Xiang, W.; Bao, Z.; Liu, C.; Deng, B. Uranium(VI) reduction by nanoscale zero-valent iron in anoxic batch systems: The role of Fe(II) and Fe(III). *Chemosphere* **2014,** *117*, 625-630.
(31) Vochten, R.; Blaton, N.; Peeters, O. Deliensite, Fe(UO 2) 2 (SO 4) 2 (OH) 2 .3H 2 O, a new ferrous uranyl sulfate hydroxyl hydrate from Mas d'Alary, Lodeve, Herault, France. *The Canadian Mineralogist* **1997,** *35*, 1021-1026.
(32) J. Plášil, J. H., V. Petříček, N. Meisser, S. J. Mills, R. Škoda, K. Fejfarová, J. Čejka, J. Sejkora, J. Hloušek, J.-M. Johannet, V. Machovič, L. Lapčák Crystal structure and formula revision of deliensite, Fe[(UO2)2(SO4)2(OH)2](H2O)7. *Mineralogical Magazine* **2012,** *76*, 2837-2860.
(33) Plá; il, J.; Kasatkin, A. V.; koda, R.; Novák, M.; Kallistová, A.; Du; ek, M.; Skála, R.; Fejfarová, K.; ejka, J.; Meisser, N.; Goethals, H.; Machovi; V.; Lap; ár, L. Leydetite, Fe(UO2)(SO4)2 (H2 O)11 , a new uranyl sulfate mineral from Mas d'Alary, Lodève, France. *Mineralogical Magazine* **2013,** *77*, 429-441.
(34) Qiu, J.; Dong, S.; Szymanowski, J. E. S.; Dobrowolska, M.; Burns, P. C. Uranyl-Peroxide Clusters Incorporating Iron Trimers and Bridging by Bisphosphonate- and Carboxylate-Containing Ligands. *Inorganic Chemistry* **2017,** *56*, 3738-3741.
(35) Dodge Cleveland, J.; Francis Arokiasamy, J., Structural characterization of a ternary Fe(III)-U(VI)-citrate complex. In *Radiochimica Acta*, 2003; Vol. 91, p 525.

(36) Basile, M.; Unruh, D. K.; Flores, E.; Johns, A.; Forbes, T. Z. Structural characterization of environmentally relevant ternary uranyl citrate complexes present in aqueous solutions and solid state materials. *Dalton Transactions* **2015,** *44*, 2597-2605.
(37) Thuery, P.; Harrowfield, J. Recent advances in structural studies of heterometallic uranyl-containing coordination polymers and polynuclear closed species. *Dalton Transactions* **2017,** *46*, 13660-13667.
(38) Jayasinghe, A. S.; Payne, M. K.; Forbes, T. Z. Synthesis and characterization of heterometallic uranyl pyridinedicarboxylate compounds. *Journal of Solid State Chemistry* **2017,** *254*, 25-31.
(39) Patel, D.; Wooles, A. J.; Hashem, E.; Omorodion, H.; Baker, R. J.; Liddle, S. T. Comments on Reactions of Oxide Derivatives of Uranium with Hexachloropropene to give UCl_4. *New J. Chem.* **2015,** *39*, 7559-7562.
(40) Wilkerson, M. P.; Burns, C. J.; Paine, R. T.; Blosch, L. L.; Andersen, R. A. Organometallic and coordination complexes. Di(μ-chloro)bis{chlorodioxobis(tetrahydrofuran)uranium(VI)}, $\{UO_2Cl_2(THF)_2\}_2$. *Inorg. Synth.* **2004,** *34*, 93-95.
(41) Bruker *APEX3* Bruker AXS Inc.: Madison, Wisconsin, USA., 2016.
(42) Sheldrick, G. M. *SADABS*, University of Göttingen, Germany, 1996.
(43) Sheldrick, G. M. SHELXT – Integrated space-group and crystal-structure determination. *Acta Cryst.* **2015,** *A71*, 3-8.
(44) Hubschle, C. B.; Sheldrick, G. M.; Dittrich, B. ShelXle: a Qt graphical user interface for SHELXL. *Journal of Applied Crystallography* **2011,** *44*, 1281-1284.
(45) McKinnon, J. J.; Jayatilaka, D.; Spackman, M. A. Towards quantitative analysis of intermolecular interactions with Hirshfeld surfaces. *Chem. Comm.* **2007**, 3814-3816.
(46) Spackman, M. A.; Jayatilaka, D. Hirshfeld surface analysis. *CrystEngComm* **2009,** *11*, 19-32.
(47) M. J. Turner, J. J. M., S. K. Wolff, D. J. Grimwood, P. R. Spackman, D. Jayatilaka and M. A. Spackman *CrystalExplorer17*, University of Western Australia, 2017.
(48) Denning, R. G. Electronic Structure and Bonding in Actinyl Ions and their Analogs. *J. Phys. Chem. A* **2007,** *111*, 4125-4143.
(49) Neidig, M. L.; Clark, D. L.; Martin, R. L. Covalency in f-element complexes. *Coord. Chem. Rev.* **2013,** *257*, 394-406.
(50) Grenthe, I.; Drożdżyński, J.; Fujino, T.; Buck, E. C.; Albrecht-Schmitt, T. E.; Wolf, S. F., Uranium. In *The Chemistry of the Actinide and Transactinide Elements*, Morss, L. R.; Edelstein, N. M.; Fuger, J., Eds. Springer Netherlands: Dordrecht, 2011; pp 253-698.
(51) Thuéry, P. 2,2'-Bipyridine and 1,10-Phenanthroline as Coligands or Structure-Directing Agents in Uranyl–Organic Assemblies with Polycarboxylic Acids. *Eur. J. Inorg. Chem.* **2013**, 4563-4573.
(52) Thuéry, P. Uranyl Ion Complexation by Citric and Citramalic Acids in the Presence of Diamines. *Inorg. Chem.* **2007,** *46*, 2307-2315.
(53) Carter, K. P.; Kalaj, M.; Cahill, C. L. Probing the Influence of N-Donor Capping Ligands on Supramolecular Assembly in Molecular Uranyl Materials. *Eur. J. Inorg. Chem.* **2016**, 126-137.
(54) Thuéry, P.; Harrowfield, J. Uranyl Ion Complexes with Long-Chain Aliphatic α,ω-Dicarboxylates and 3d-Block Metal Counterions. *Inorg. Chem.* **2016,** *55*, 2133-2145.
(55) Alcock, N. W.; Flanders, D. J.; Brown, D. Actinide structural studies. Part 7. The crystal and molecular structures of (2,2'-bipyridyl)dinitratodioxo-uranium(VI) and -neptunium(VI),

and diacetato-(2,2'-bipyridyl)dioxo-uranium(VI) and -neptunium(VI). *J. Chem. Soc. Dalton Trans.* **1985**, 1001-1007.
(56) Haiges, R.; Vasiliu, M.; Dixon, D. A.; Christe, K. O. The Uranium(VI) Oxoazides $[UO_2(N_3)_2{\cdot}CH_3CN]$, $[(bipy)_2(UO_2)_2(N_3)_4]$, $[(bipy)UO_2(N_3)_3]^-$, $[UO_2(N_3)_4]^{2-}$, and $[(UO_2)_2(N_3)_8]^{4-}$. *Chem. Eur. J.* **2017,** *23*, 652-664.
(57) Thuéry, P.; Harrowfield, J. Complexation of Uranyl Ion with Sulfonates: One- to Three-Dimensional Assemblies with 1,5- and 2,7-Naphthalenedisulfonates. *Eur. J. Inorg. Chem.* **2017**, 979-987.
(58) Carter, K. P.; Kalaj, M.; Kerridge, A.; Ridenour, J. A.; Cahill, C. L. How to Bend the Uranyl Cation via Crystal Engineering. *Inorganic Chemistry* **2018**.
(59) Hayton, T. W. Understanding the origins of Oyl-U-Oyl bending in the uranyl (UO22+) ion. *Dalton Transactions* **2018,** *47*, 1003-1009.
(60) *The Importance of Pi-Interactions in Crystal Engineering: Frontiers in Crystal Engineering*. John Wiley & Sons Ltd: Chichester, 2012.
(61) Spackman, M. A.; McKinnon, J. J. Fingerprinting intermolecular interactions in molecular crystals. *CrystEngComm* **2002,** *4*, 378-392.
(62) Collins, R. N.; Rosso, K. M. Mechanisms and Rates of U(VI) Reduction by Fe(II) in Homogeneous Aqueous Solution and the Role of U(V) Disproportionation. *J. Phys. Chem. A* **2017,** *121*, 6603-6613.
(63) Taylor, S. D.; Marcano, M. C.; Rosso, K. M.; Becker, U. An experimental and ab initio study on the abiotic reduction of uranyl by ferrous iron. *Geochim. Cosmochim. Acta* **2015,** *156*, 154-172.
(64) Surbella Iii, R. G.; Andrews, M. B.; Cahill, C. L. Self-assembly of $[UO_2X_4]^{2-}$ (X=Cl, Br) dianions with γ substituted pyridinium cations: Structural systematics and fluorescence properties. *J. Solid State Chem.* **2016,** *236*, 257-271.
(65) Schnaars, D. D.; Wilson, R. E. Lattice Solvent and Crystal Phase Effects on the Vibrational Spectra of $UO_2Cl_4^{2-}$. *Inorg. Chem.* **2014,** *53*, 11036-11045.
(66) Deifel, N. P.; Cahill, C. L. Supramolecular chemistry with uranyl tetrahalide ($[UO_2X_4]^{2-}$) anions. *C. R. Chim.* **2010,** *13*, 747-754.
(67) Yao, A.; Chu, T. Uranium dioxide in Fe(III)-containing ionic liquids with DMSO: Dissolution, separation, and structural characterization. *J. Nucl. Mat.* **2016,** *480*, 301-309.
(68) Dao Feng, X.; Xiang Shi, T.; Si Wei, Z.; Yu, H.; Kai Bei, Y.; Wen Xia, T. Synthesis, crystal structure and properties of $[Fe_2O(bipy)_4Cl_2](ClO_4)_2 \cdot 0.25CH_3CN \cdot 0.25CH_3OH \cdot 0.25H_2O$, a μ-Oxo diiron(III) complex. *Polyhedron* **1998,** *17*, 2095-2100.
(69) Oyaizu, K.; Listiani Dewi, E.; Tsuchida, E. A μ-oxo diiron(III) complex with a short Fe–Fe distance: crystal structure of (μ -oxo)bis[N,N′ -o-phenylenebis(salicylideneiminato)iron(III)]. *Inorg. Chim. Acta* **2001,** *321*, 205-208.
(70) Maher, K.; Bargar, J. R.; Brown, G. E. Environmental Speciation of Actinides. *Inorg. Chem.* **2013,** *52*, 3510-3532.
(71) Natrajan, L. S.; Swinburne, A. N.; Andrews, M. B.; Randall, S.; Heath, S. L. Redox and Environmentally Relevant Aspects of Actinide(IV) Coordination Chemistry. *Coord. Chem. Rev.* **2014,** *266–267*, 171-193.
(72) Neck, V.; Kim, J. I. Solubility and hydrolysis of tetravalent actinides. *Radiochim. Acta* **2001,** *89*, 1-16.
(73) Gans, P.; Smith, B. C. Reactions of uranium tetrachloride with 2,2'-bipyridyl and o-phenanthroline. *J. Chem. Soc.* **1964**, 4177-4179.

(74) Wacker, J. N.; Vasiliu, M.; Huang, K.; Baumbach, R. E.; Bertke, J. A.; Dixon, D. A.; Knope, K. E. Uranium(IV) Chloride Complexes: UCl_6^{2-} and an Unprecedented $U(H_2O)_4Cl_4$ Structural Unit. *Inorg. Chem.* **2017,** *56*, 9772-9780.
(75) Bossé, E.; Den Auwer, C.; Berthon, C.; Guilbaud, P.; Grigoriev, M. S.; Nikitenko, S.; Naour, C. L.; Cannes, C.; Moisy, P. Solvation of UCl_6^{2-} Anionic Complex by $MeBu_3N^+$, $BuMe_2Im^+$, and $BuMeIm^+$ Cations. *Inorg. Chem.* **2008,** *47*, 5746-5755.
(76) Minasian, S. G.; Boland, K. S.; Feller, R. K.; Gaunt, A. J.; Kozimor, S. A.; May, I.; Reilly, S. D.; Scott, B. L.; Shuh, D. K. Synthesis and Structure of $(Ph_4P)_2MCl_6$ (M = Ti, Zr, Hf, Th, U, Np, Pu). *Inorg. Chem.* **2012,** *51*, 5728-5736.
(77) Ikeda-Ohno, A.; Hennig, C.; Tsushima, S.; Scheinost, A. C.; Bernhard, G.; Yaita, T. Speciation and Structural Study of U(IV) and -(VI) in Perchloric and Nitric Acid Solutions. *Inorganic Chemistry* **2009,** *48*, 7201-7210.